# Thermal Characteristic Analysis of a High-Precision Centerless Grinding Machine for Machining Ferrules

**Seok-Il Kim[1, #] and Jae-Wan Cho[2]**

1 School of Aerospace and Mechanical Engineering, Hankuk Aviation University, Goyang-Si, Gyeonggi-Do, South Korea
2 Graduate School, Hankuk Aviation University, Goyang-Si, Gyeonggi-Do, South Korea
# Corresponding author: E-mail: sikim@hau.ac.kr; Tel: +82-2-300-0176; Fax: +82-2-3158-4231

KEYWORDS : High-precision centerless grinding machine, Thermal characteristic analysis, Grinding wheel, Regulating wheel, Hydrostatic bearing, Ferrule

*The outer diameter finishing grinding process required for ferrules, which are widely used as fiber optic connectors, is carried out by high-precision centerless grinding machines. In this study, the thermal characteristics of such a machine, for example, the temperature distribution, temperature rise, and thermal deformation, were estimated based on a virtual prototype and the heat generation rates of heat sources related to normal operating conditions. The prototype consisted of a concrete-filled bed, hydrostatic grinding wheel (GW) and regulating wheel (RW) spindle systems, a hydrostatic RW feed mechanism, a RW swivel mechanism, and on-machine GW and RW dressers. The reliability of the predicted results was demonstrated using temperature characteristics measured from a physical prototype. The predicted and measured results indicated that this particular high-precision centerless grinding machine had very stable thermal characteristics.*

Manuscript received: May 8, 2006 / Accepted: May 12, 2006

## 1. Introduction

Ferrules, which are widely used as fiber optic connectors, require a high-precision outer diameter grinding process to improve their transmission efficiency and thus the quality of optical communication systems.[1] In general, ferrules are made from zirconia ($ZrO_2$), which is a ceramic material. Most of the required tolerances for ferrules are less than 1 μm, and their outer diameter, concentricity, roundness, and surface roughness are very strictly regulated.

The preferred strategy to effectively perform the outer diameter finishing grinding process for ferrules is the use of centerless grinding machines, which are able to manufacture high-precision products regardless of operator skills.[2,3] Because the product precision is totally dependent on the machining accuracies of the machines, the development of a high-precision centerless grinding machine is required to achieve the required outer diameter tolerances when grinding ferrules. To realize such a machine, the thermal stability of existing machines must be enhanced as well as their structural stability.

Cho *et al.*[4] investigated the specifications and functions required to realize a high-precision centerless grinding machine, while Lee *et al.*[5] manufactured and evaluated the required on-machine wheel dressing system. Park *et al.*[6] experimentally estimated the stiffness, position accuracy, and repeatability of a hydrostatic feed system for a centerless grinding machine and demonstrated its potential applicability for high-precision machining. Kim *et al.*[7] estimated the feasibility of a structural design based on the structural analysis and experimental results of a table feed system for a high-precision centerless grinding machine, which consisted of a concrete-filled bed, a hydrostatic guideway, and a servomotor-ball screw driving mechanism. They identified the causes of structural stiffness deterioration, which are difficult to elucidate experimentally, by investigating the effects of the structural elements on the axial and vertical stiffness values of the feed system. Kim and Cho[8] analyzed the influences of the machine weight and grinding forces on the structural deformation based on a virtual prototype of a centerless grinding machine. They also evaluated the loop stiffness values based on the relative displacements between the grinding wheel (GW) and regulating wheel (RW) caused by the grinding forces and demonstrated that the use of a concrete-filled bed had a considerable effect on the structural stiffness and accuracy of the machine by comparing the structural characteristics of concrete-filled and unfilled beds. However, these studies were only concerned with the structural aspects of grinding machines; a thermal characteristic analysis study that systematically identifies and estimates problems in the thermal design has not yet been performed.

In this study, the effects of thermal characteristics on the grinding performance of a high-precision centerless grinding machine were estimated in the design stage. The thermal characteristics of such a machine, for example, the temperature distribution, temperature rise, and thermal deformation, were analyzed based on a virtual prototype that consisted of a concrete-filled bed, hydrostatic GW and RW spindle systems, a hydrostatic RW feed mechanism, a RW swivel mechanism, and on-machine GW and RW dressers. In addition to the cooling effects caused by the convection heat transfer at the machine surface and coolant path, the heat generation rates of heat sources, such as the hydrostatic bearings of the GW and RW spindle systems, belt pulleys, pulley-support bearings, and motors, were considered to

perform the thermal characteristic analysis. The reliability of the predicted results was demonstrated using the temperature characteristics measured from a physical prototype. A comparison of the predicted and measured results demonstrated that the high-precision centerless grinding machine had very stable thermal characteristics.

## 2. Structure and Specifications of the High-Precision Centerless Grinding Machine

### 2.1 Grinding Machine

The basic structure of the high-precision centerless grinding machine is presented in Fig. 1. The GW spindle head was mounted directly on the left portion of bed and the RW spindle head, which contained a swivel head that regulated the RW setting angle to determine the workpiece feed rate, was mounted on the feed table. To simplify the machine structure and to enhance the efficiency of the grinding operation, the on-machine GW and RW dressers were mounted behind the GW and RW spindle heads, respectively, and concrete was used to fill the steel bed to obtain a stiff machine structure.

The width and diameter of the GW were set to 150 and 250 mm, respectively, to grind ten ferrules with the specifications shown in Table 1. The width and diameter of the RW were set to 180 and 205 mm, respectively, to ensure sufficient guiding accuracy when the ferrules entered the grinding process. The GW was made from diamond since the ferrules were composed of zirconia.

### 2.2 Spindle Systems

The spindle systems of the high-precision centerless grinding machine were separated into GW and RW components. Hydrostatic bearings were used for the spindle because the roundness and surface roughness of the ferrules are greatly influenced by the rotational accuracy of the spindle systems. The stiff spindle systems required to minimize the displacement of the wheels due to the grinding load were realized by installing the GW and RW between left and right hydrostatic journal bearings. Fig. 2 shows a schematic diagram of the hydrostatic journal bearings, and the design specifications are listed in Table 2. The same information for the hydrostatic thrust bearings can be found in Fig. 3 and Table 3.[9]

### 2.3 Feed System

The outer diameter and concentricity of a ferrule are greatly influenced by the axial stiffness and feed accuracy of the RW table feed system due to the grinding principles of the high-precision centerless grinding machine. Therefore, a hydrostatic guideway and a servomotor-ball screw driving mechanism were used in the feed system. Since most of the grinding load is applied in the axial direction of the RW table feed system, the axial stiffness of the feed system has to be sufficient to achieve the required ferrule tolerances. By considering these factors, a NSK PFT 4006-7.5 with an oversize ball preload was selected as the ball screw for the RW table feed system. Four angular contact ball bearings, NSK 30TAC62, were installed on the servomotor side to act as ball screw support bearings.

The vertical stiffness of the hydrostatic guideway was designed by considering the weights of the RW spindle head and RW dresser mounted on the feed table, as shown in Fig. 1. The horizontal stiffness of the hydrostatic guideway was designed by considering the fact that smaller feed table yaw errors give rise to better ferrule tolerances. Therefore, to improve the stiffness and ease of assembly of the hydrostatic guideway, a reverse confining hydrostatic guideway, in which the rails wrap the double-pad hydrostatic bearings as shown in Fig. 4, was introduced. To improve the feed accuracy, countermeasures for minimizing the elastic deformation of the

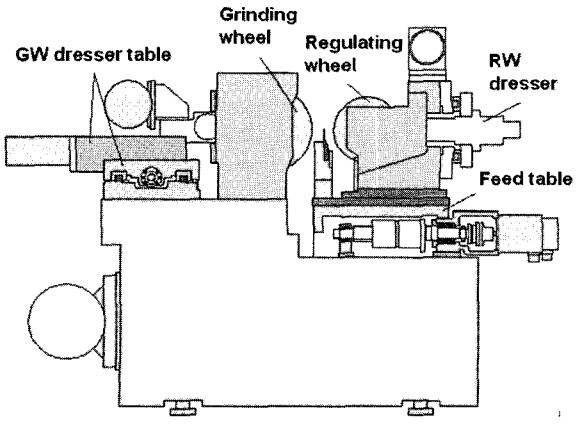


Fig. 1 Schematic diagram of a centerless grinding machine

Table 1 Ferrule specifications

| | | | |
|---|---|---|---|
| Dimensions | 2.5 × 10.5 mm | Accuracy | 60.5 μm |
| Material | $ZrO_2$ | Roundness | 0.5 μm |
| Roughness | 0.05 μm $R_a$ | Concentricity | 1.0 μm |

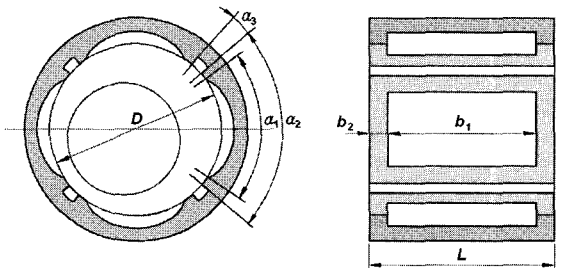


Fig. 2 Schematic diagram of the hydrostatic journal bearings

Table 2 Specifications of the hydrostatic journal bearings

| Specifications | GW spindle | RW spindle |
|---|---|---|
| Diameter/Length *D*, *L* | 60, 60 mm | 50, 50 mm |
| Angle $\alpha_1$, $\alpha_2$, $\alpha_3$ | 63°, 86.18°, 3.82° | 62.5°, 80.8°, 9.2° |
| Axial length $b_1$, $b_2$ | 48, 6 mm | 40, 5 mm |
| Bearing clearance | 20 μm | 20 μm |
| Stiffness | 241 N/μm | 163 N/μm |
| Flow rate of oil | 0.72 ℓ/min | 0.82 ℓ/min |
| Supply pressure | 2 MPa | |
| Density | 822 kg/m$^3$ | |
| Specific heat | 1,800 J/kg°C | |
| Dynamic viscosity | 5 cSt (40 °C) | |

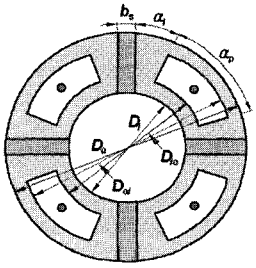


Fig. 3 Schematic diagram of the hydrostatic thrust bearings

Table 3 Specifications of the hydrostatic thrust bearings

| Specifications | GW spindle | RW spindle |
|---|---|---|
| $D_i$, $D_{io}$, $D_{oi}$, $D_o$ | 64, 67, 77, 80 mm | 54, 58, 68, 72 mm |
| Angle $\alpha_l$, $\alpha_p$ | 11.91°, 63° | 11.68°, 63° |
| Width $b_s$ | 4 mm | 4 mm |
| Bearing clearance | 20 μm | 20 μm |
| Stiffness | 150 N/μm | 143 N/μm |
| Flow rate of oil | 2.80 ℓ/min | 1.53 ℓ/min |
| Supply pressure | 2 MPa | |
| Density | 822 kg/m$^3$ | |
| Specific heat | 1,800 J/kg°C | |
| Dynamic viscosity | 5 cSt (40 °C) | |

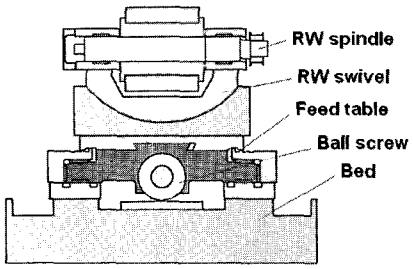


Fig. 4 Hydrostatic guideway structure

Table 4 Specifications of the hydrostatic guideway

| Specifications | Horizontal | Vertical |
|---|---|---|
| Number of pads | 6 | 12 |
| Pad dimensions | 120×32 mm | 120×32 mm |
| Bearing clearance | 25 μm | 25 μm |
| Static stiffness | 480 N/μm | 960 N/μm |
| Flow rate of oil | 0.65 ℓ/min | 1.30 ℓ/min |
| Supply pressure | 1 MPa | |
| Density | 822 kg/m$^3$ | |
| Specific heat | 1,800 J/kg°C | |
| Dynamic viscosity | 5 cSt (40 °C) | |

guideway structure due to the recess pressure of the hydrostatic bearings were required in addition to the left–right symmetric structure design of the feed system. The design specifications of the hydrostatic guideway that were established based on these concepts are presented in Table 4.[9]

## 3. Thermal Characteristic Analysis of the High-Precision Centerless Grinding Machine

### 3.1 Virtual Prototype (Finite Element Model)

A virtual prototype of the high-precision centerless grinding machine was constructed to estimate its thermal characteristics, as shown in Fig. 5. The principal structural modules of the virtual prototype are presented in Fig. 6 to better explain the construction of the centerless grinding machine. The virtual prototype consisted of 79,319 nodes and 94,867 solid elements.

The GW and RW spindles and the bed were made of steel (SS440, SCM435), while the GW and RW spindle housings, the GW and RW dresser housings, and the feed table and rails of the RW table feed system were made of cast iron (GC300). Concrete was used to fill the bed. The material properties are given in Table 5. The mass of each structural module illustrated in Fig. 6 was estimated as follows: 727 kg for the steel bed, 791 kg for the concrete, 287 kg for the RW table feed mechanism (table, rails, ball screw, bracket, and servomotor), 344 kg for the GW spindle head (spindle and housing), 294 kg for the RW spindle head (spindle, housing, and motor), 351 kg for the GW dresser, 27 kg for the RW dresser, and 84 kg for the GW spindle motor. The estimated total mass of the high-precision centerless grinding machine was 2,905 kg.

When ferrules were ground, 37.5 ℓ /min of coolant was supplied to the grinding zone via injection nozzles as shown in Fig. 5. The bed was also cooled by 37.5 ℓ /min of another coolant running from the four corners of the bed. Positions 1 and 2 in the figure refer to the location of the injection nozzles and the spot located under the grinding zone, respectively. Positions 3, 4, 5, and 6 give the four corners of the bed, and positions 7 and 8 indicate the confluence and outlet of the coolant, respectively.

### 3.2 Heat Source and Heat Transfer Rate

To perform the thermal characteristic analysis of the high-precision centerless grinding machine, the heat generation rates of the heat sources, such as the hydrostatic bearings of the GW and RW spindle systems, belt pulleys, pulley support bearings, and motors,

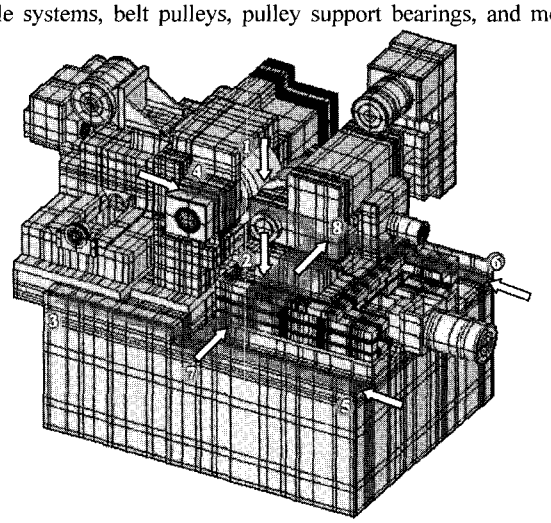

Fig. 5 Virtual prototype and coolant path of the grinding machine

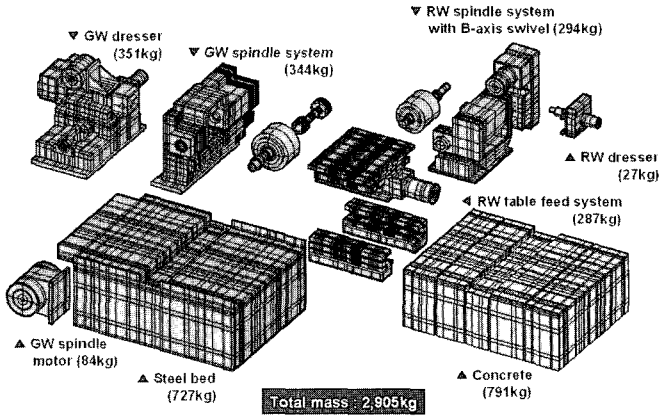


Fig. 6 Structural modules of the virtual prototype

Table 5 Material properties used for the virtual prototype

| Material | Density (kg/m$^3$) | Young's modulus (GPa) | Poisson's ratio | Thermal conductivity (W/m°C) | Thermal expansion (μm/°C) | Specific heat (J/kg°C) |
|---|---|---|---|---|---|---|
| SS400 | 7,870 | 205.0 | 0.30 | 42.7 | 10.4 | 473 |
| SCM435 | 7,850 | 205.0 | 0.28 | 42.7 | 11.2 | 477 |
| SCM415 | 7,850 | 205.0 | 0.28 | 44.5 | 11.2 | 475 |
| GC300 | 7,300 | 90.0 | 0.25 | 55.8 | 17.1 | 565 |
| Concrete | 2,320 | 27.0 | 0.18 | 1.0 | 10.5 | 657 |
| GW | 3,800 | 50.0 | 0.30 | 1.0 | 7.6 | 664 |
| RW | 1,150 | 2.0 | 0.40 | 0.4 | 80.0 | 2,092 |
| Al | 2,700 | 70.0 | 0.33 | 205.0 | 24.0 | 900 |
| SUJ2 | 7,860 | 205.8 | 0.30 | 41.9 | 12.5 | 473 |
| Fe–Si | 7,700 | 21.0 | 0.30 | 42.7 | 15.0 | 477 |
| Cu | 8,930 | 123.0 | 0.34 | 397.5 | 16.5 | 385 |

were considered in addition to the cooling effects caused by the convection heat transfer at the machine surface and along the coolant path.

In general, the heat generated in the hydrostatic bearings can be separated into two sources: the heat caused by the shearing of the oil film and the heat caused by the oil pressure drop. When the coolant is discharged to the outside, heat is discharged with it. Thus, the heat, which contributes to the temperature rise of the machine structure, can be obtained by extracting the heat discharged by the coolant from the heat generated in the bearing.

Hydrostatic thrust bearings have very small heat transfer rates because the heat discharged by the coolant is great due to the large flow rate. The heat generated by the friction between the V-belt and pulley and the heat generated in the pulley support bearings contribute directly to the temperature rise of the machine structure.

Table 6 Heat transfer rates used for the virtual prototype

| Heat sources | | Heat transfer rate (W) |
|---|---|---|
| GW spindle | Hydrostatic journal bearing | 37.0 |
| | Hydrostatic thrust bearing | 1.0 |
| | Pulley support bearing | 1.2 |
| | Belt pulley | 27.0 |
| | Spindle motor | 19.9 |
| RW spindle | Hydrostatic journal bearing | 12.0 |
| | Hydrostatic thrust bearing | 0.0 |
| | Spindle motor | 0.9 |
| RW guideway | Horizontal hydrostatic guideway | 0.1 |
| | Vertical hydrostatic guideway | 0.2 |

Because the RW table feed system maintains a rest state during the grinding process, the heat generated in the ball screw nut and support bearing is negligible. The heat generated in the hydrostatic guideway is only due to the oil pressure drop, and most of the heat is discharged to the outside by the coolant.

In this study, it was assumed that the ambient temperature remained constant, and the coolant temperature and the temperature of the oil supplied to the hydrostatic bearings and guideway were equal to the ambient temperature. The GW and RW spindle speeds were 2,300 and 35 rpm, respectively. The heat transfer rates used for the virtual prototype under these operating conditions are listed in Table 6.

### 3.3 Temperature Rise

The temperature rise of the high-precision centerless grinding machine is illustrated in Fig. 7 in isometric view, and the temperature rise of the GW and RW spindle systems are illustrated in Fig. 8(a) and (b) in sectional views. The predicted maximum temperature rise of the high-precision centerless grinding machine was 14.3 °C, which occurred at the belt pulley of the GW spindle system. The temperature rise was relatively high in the GW and RW spindle systems where the heat sources were concentrated. The temperature rise of the GW spindle system was higher than that of the RW spindle

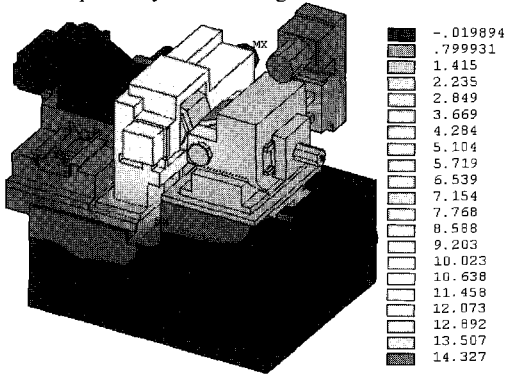


Fig. 7 Temperature distribution of the virtual prototype (isometric view)

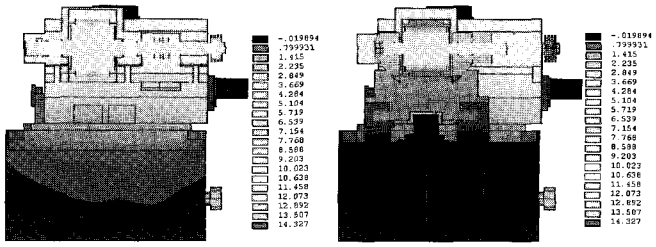

(a) GW spindle system (b) RW spindle system

Fig. 8 Temperature distribution of the virtual prototype (sectional views)

Table 7 Temperature rise of the virtual prototype at different locations

| Positions | GW spindle | RW spindle |
|---|---|---|
| Pocket of journal bearing (left) | 6.1 °C | 2.4 °C |
| Center of wheel spindle | 5.6 °C | 3.1 °C |
| Pocket of journal bearing (right) | 5.5 °C | 2.2 °C |
| Outer race of ball bearing (left) | 4.1 °C | - |
| Outer race of ball bearing (right) | 4.7 °C | - |

system because the heat transfer rates of the heat sources of the GW spindle system were larger, as shown in Table 6. The temperature rise at the principal positions of the GW and RW spindle systems are given in Table 7.

The temperature rise of the GW spindle system shown in Fig. 8(a) indicates that the heat generated in the belt pulley contributes somewhat to the temperature rise of the pulley support bearings but does not diffuse toward the overall GW spindle system. The temperature rise of the GW spindle system, except in the neighborhood of the belt pulley, was mainly caused by the heat generated in the hydrostatic journal bearings. The temperature rise of the RW spindle system was also largely influenced by the heat generated in the hydrostatic journal bearings, as shown in Fig. 8(b).

The temperature distribution of a physical prototype was measured to verify the reliability of the thermal characteristic analysis. The physical prototype and the experimental apparatus are shown in Fig. 9. The warming-up time of the physical prototype was 4 hours, and the temperature was measured while ferrules were ground. The

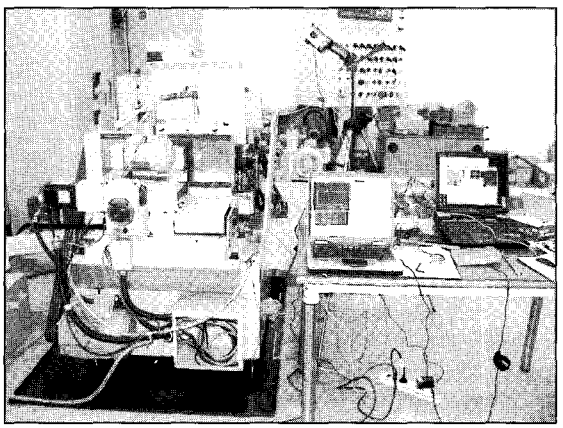

Fig. 9 Physical prototype and experimental apparatus

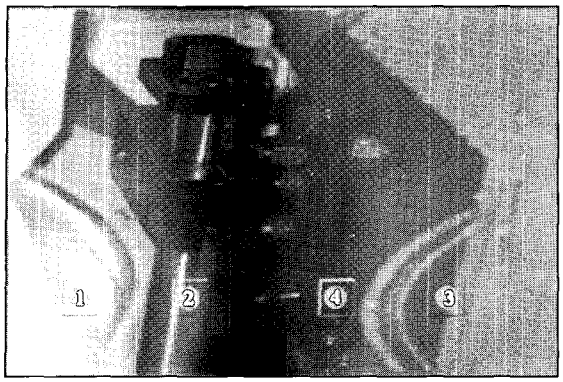


Fig. 10 Measurement positions and temperature distribution

Table 8 Comparison of the temperature rise at different locations

| Positions | Predicted (°C) | Measured (°C) |
|---|---|---|
| ① Inner point of GW | 5.6 | 5.5 |
| ② Outer point of GW | 1.5 | 1.6 |
| ③ Inner point of RW | 3.2 | 3.5 |
| ④ Outer point of RW | 0.8 | 0.9 |

temperature distribution of the grinding zone was measured by a thermal image camera (IRI1001E, IRISYS), and the temperature of the coolant was measured at the eight positions shown in Fig. 5 using T-type thermocouples. The temperature rise of the coolant differed according to the measurement position, but only ranged between 0.0 and 0.2 °C. This fact demonstrated that the heat generated when ferrules were ground was low and the temperature of the coolant path was also low. As a result, we could confirm that the ambient temperature and the coolant temperature remained constant at about 16 °C during the temperature measurements.

Fig. 10 shows a thermal image of the temperature distribution in the grinding zone, and Table 8 lists the predicted and measured temperature rise of the GW and RW at the measurement positions indicated in Fig. 10. The temperature rise of the GW was greater than that of the RW because the overall heat transfer from the GW spindle system was higher. Since the difference between the predicted and measured results was small, the thermal characteristic analysis of the high-precision centerless grinding machine was deemed accurate.

### 3.4 Thermal Deformation

A thermal deformation analysis of the high-precision centerless grinding machine was performed based on the predicted temperature rise. This analysis focused on identifying the relative thermal displacement between the GW and RW, which is closely related to the machining accuracy. The thermal deformation of the high-precision centerless grinding machine is illustrated in Fig. 11 in an isometric view, and the thermal deformation of the GW and RW spindle systems is illustrated in Fig. 12(a) and (b) in sectional views. The horizontal and vertical thermal deflections of the GW and RW spindles are given in Figs. 13 and 14, respectively.

Figs. 11 and 12 show that the thermal deformation of the GW spindle system, in which the strong heat sources were concentrated, was relatively large. The predicted maximum thermal deformation of the high-precision centerless grinding machine was 44.0 μm, which occurred in the upper portion of the housing of the GW spindle system.

The horizontal thermal deflections of the GW and RW spindles were 4.4 to 8.9 μm and −0.4 to 3.7 μm, as shown in Fig. 13, and the vertical thermal deflections of the GW and RW spindles were 11.3 to 21.6 μm and 5.2 to 8.3 μm, as shown in Fig. 14. However, the deviation of the thermal deflection of the overall spindle does not affect the machining accuracy; it is the deviation of the thermal deflection of the GW and RW mounts (indicated by the dotted lines in Figs. 13 and 14) that is important. Because the horizontal thermal deflections of the GW and RW mounts were 7.9 to 8.7 μm and −0.4 to −0.2 μm, the relative horizontal thermal displacement between the

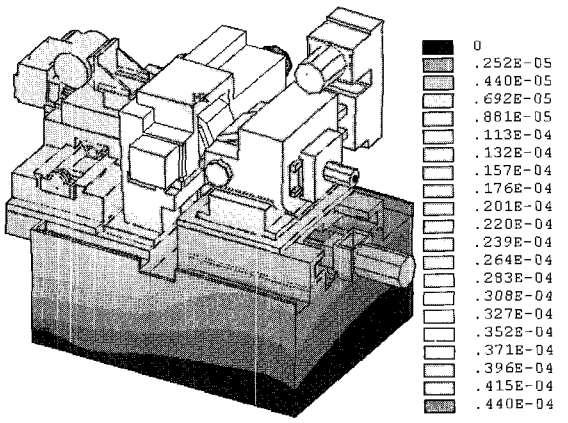


Fig. 11 Thermal deformation of the virtual prototype (isometric view)

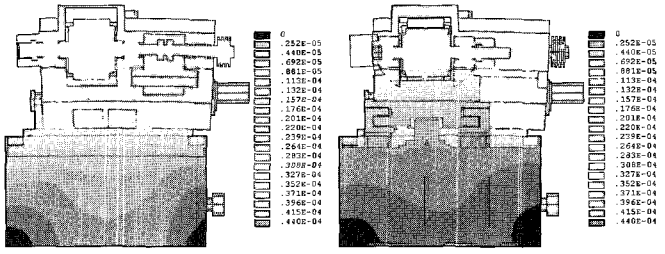

(a) GW spindle system (b) RW spindle system

Fig. 12 Thermal deformation of the virtual prototype (sectional views)

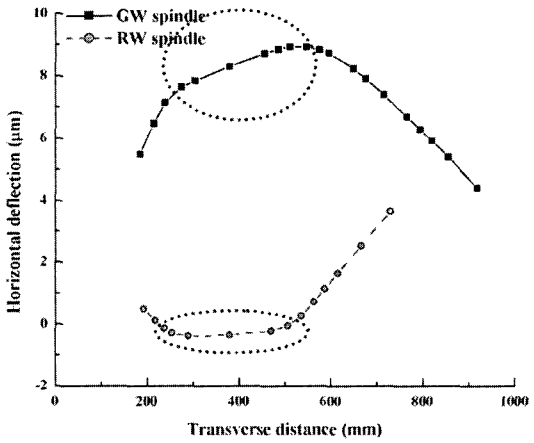


Fig. 13 Horizontal thermal deflection of the GW and RW spindles

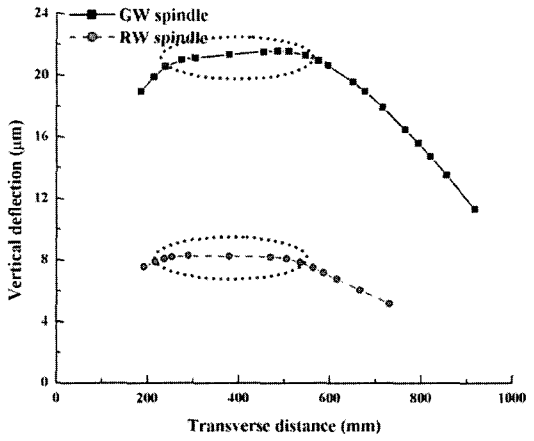


Fig. 14 Vertical thermal deflection of the GW and RW spindles

GW and RW was estimated to be 8.3 to 8.9 μm. Since the vertical thermal deflections of the GW and RW mounts were 21.1 to 21.5 μm and 8.2 to 8.3 μm, respectively, the relative vertical thermal displacement between the GW and RW was estimated to be 12.9 to 13.2 μm. Therefore, since the deviation of the relative horizontal and vertical thermal displacements between the GW and RW were 0.6 and 0.3 μm, respectively, the machining accuracy deterioration caused by the thermal deformation of the high-precision centerless grinding machine was predicted to be very small.

## 4. Conclusions

In this study, a thermal characteristic analysis and evaluation were performed under ferrule grinding conditions (with a GW spindle speed of 2,300 rpm and a RW spindle speed of 35 rpm) using a virtual prototype of a high-precision centerless grinding machine with hydrostatic bearing-based GW and RW spindle systems and a hydrostatic guideway-based feed system. The reliability of the thermal characteristic analysis was demonstrated with temperature distribution measurements on a physical prototype obtained from a thermal image camera and T-type thermocouples. The following conclusions were drawn.

1) The maximum temperature rise of the high-precision centerless grinding machine was 14.3 °C, which occurred at the belt pulley of the GW spindle system. The heat generated in the belt pulley contributed somewhat to the temperature rise of the pulley support bearings, but did not diffuse toward the overall GW spindle system.
2) The temperature rise of the GW spindle system, except in the neighborhood of the belt pulley, was mainly caused by the heat generated in the hydrostatic journal bearings. The temperature rise of the RW spindle system was also largely influenced by the heat generated in the hydrostatic journal bearings.
3) The maximum thermal deformation of the high-precision centerless grinding machine was 44.0 μm, which occurred in the upper portion of the housing of the GW spindle system. The thermal deformation of the GW spindle system, in which the strong heat sources were concentrated, was relatively large.
4) Because the deviations of the relative horizontal and vertical thermal displacements between the GW and RW were 0.6 μm and 0.3 μm, respectively, the machining accuracy deterioration caused by the thermal deformation of the high-precision centerless grinding machine was predicted to be very small.

## ACKNOWLEDGEMENT

This research was supported by the Middle Term Stronghold Technology Development Program of the Korean Ministry of Commerce, Industry and Energy.

## REFERENCES

1. Takeuchi, Y., Mitachi, S. and Nagase, R., "High-strength class-ceramic ferrule for SC-type single-mode optical fiber connector," IEEE Photonics Technology Letters, Vol. 9, No. 11, pp. 1502-1504, 1997.
2. Rowe, W. B., Spraggett, S., Gill, R. and Davies, B. J., "Improvements in centreless grinding machine design," Annals of the CIRP, Vol. 36, No. 1, pp. 207-210, 1987.
3. Rowe, W. B., Miyashita, M. and Koenig, W., "Centerless grinding research and its application in advanced manufacturing technology," Annals of the CIRP, Vol. 38, No. 2, pp. 617-626, 1989.
4. Cho, S. J., Kim, H. G., Ebihara, T. and Tuskisima, H., "The study on the development of ultra precision centerless grinder," Journal of KSPE, Vol. 20, No. 6, pp. 11-14, 2003.
5. Lee, E. S., Cho, C. R. and Park, B. J., "Development of rotary diamond dressing system of centerless grinder for ferrule grinding," Journal of KSPE, Vol. 20, No. 6, pp. 15-19, 2003.
6. Park, C. H., Hwang, J. H. and Cho, S. J., "A study on the feeding system of centerless grinder for machining the ferrule," Proc. of KSPE, pp. 65-69, 2002.
7. Kim, S. I., Park, C. H. and Cho, S. J., "Structural characteristic analysis on the hydrostatic guide way and feeding system of a high-precision centerless grinder for machining ferrules," Trans. of KSME (A), Vol. 28, No. 7, pp. 896-903, 2004.
8. Kim, S. I. and Cho, J. W., "Structural characteristic analysis of a high-precision centerless grinding machine with a concrete-filled bed," Journal of KSPE, Vol. 22, No. 2, pp. 172-179, 2005.
9. Park, C. H., "Design and performance evaluation on the motion elements of centerless grinder," 3rd Mid-Evaluation Workshop of Intelligent Grinding System, 2004.